

## Study on reaction mechanisms of iron matrix composites reinforced with in situ Al<sub>2</sub>O<sub>3</sub> particles reacted by Al-Fe<sub>2</sub>O<sub>3</sub>-Fe system

Chengyan Zhu, Jie Jiang, Heguo Zhu \*

College of Materials Science and Engineering, Nanjing University of Science and Technology, Nanjing, 210094; P. R. China

**Abstract.** Iron matrix composites reinforced with Al<sub>2</sub>O<sub>3</sub> particles were fabricated in situ through exothermic dispersive (XD) reaction from a powder mix of pure elements Fe, Al and Fe<sub>2</sub>O<sub>3</sub>. The fabrication and reaction mechanisms were investigated by using X-ray diffraction (XRD), scanning electron microscopy (SEM), X-ray energy dispersive spectroscopy (EDS) and differential scanning calorimetry (DSC) analysis. The reaction between Al and Fe<sub>2</sub>O<sub>3</sub> was found to occur in three steps. Their activation energies are 203.8 kJ/mol, 1100.9 kJ/mol and 380 kJ/mol, respectively. DSC analysis shows that the reaction peak shifts to a higher temperature with an increase in the heating rate. When the heating rate is 10 K/min, the rates of the three reactions exhibit a similar trend, i.e., the reaction rate is very slow at the start, and then it increases rapidly, finally it becomes slow again. Their reaction times are 456, 672 and 650 s, respectively.

### 1. INTRODUCTION

Iron matrix composites (MMCs) exhibit many attractive features, such as good thermal and electrical conductivities, high strength and fracture toughness and excellent wear resistance. *In situ* iron matrix composites are new additions, whose reinforcements are formed through one or more *in situ* reactions among raw materials. They have attracted considerable attention in recent years owing to clean reinforcement/matrix interface, high thermal stability, good isotropic properties and low fabrication costs [1,2].

Alumina ceramic (Al<sub>2</sub>O<sub>3</sub>) particles possess outstanding physical and mechanical properties, for example, high modulus and hardness, low density, high melting temperature (2323K), excellent oxidation resistance and thermal stability in metal melt. They are considered to be one of the best reinforcements in the fabrication of metal matrix composites [3]. Recently, iron matrix composites reinforced with TiC particles were synthesized, and their mechanical properties and wear resistance were studied [4]. In contrast, reports on Al<sub>2</sub>O<sub>3</sub> particles reinforced Fe-based composites are very limited. Georgioua *et al.* [5] prepared a nanostructured cermet coating consisting of alumina particles dispersed in a Fe–Cu–Al matrix by supersonic spraying, and identified a strong effect of processing parameters and chemical composition of the powders on the structural and mechanical characteristics of the resulting (Fe–Cu–Al) + Al<sub>2</sub>O<sub>3</sub> cermet. Accordingly, a ‘structure–property’ relationship was established for this type of nanostructured cermet coatings. In another study, Al<sub>2</sub>O<sub>3</sub> particles were mixed with Fe<sub>3</sub>Al powders

and then sintered at 1373K, and resultant iron based composites have fine grain size and high hardness [6]. Babakhani *et al.* [7] fabricated iron–alumina composite foams through a combination of combustion synthesis (CS) and spark plasma sintering (SPS). They found that applying pulsed electric current to the powder mix led to the formation of Al<sub>2</sub>O<sub>3</sub> through a highly exothermic reaction between Al and Fe<sub>2</sub>O<sub>3</sub>, i.e.,  $X\text{Fe} + 2\text{Al} + \text{Fe}_2\text{O}_3 = \text{Al}_2\text{O}_3 + (X+2)\text{Fe}$ . They also demonstrated that the time to reach the maximum combustion temperature increased with increasing X.

In this paper, *in situ* Fe-based composites reinforced with Al<sub>2</sub>O<sub>3</sub> particles were prepared, for the first time, from Fe-Fe<sub>2</sub>O<sub>3</sub>-Al powder mixtures through exothermic dispersive (XD) synthesis. The reaction process was explored and clarified by using differential scanning calorimetry (DSC), X-ray diffraction (XRD), scanning electron microscopy (SEM) and energy dispersive spectroscopy (EDS), assisted by thermodynamic analysis.

### 2. EXPERIMENTS PROCEDURES

#### 2.1. Materials

Pure Fe (40-50 μm), Fe<sub>2</sub>O<sub>3</sub> (30-50 μm) and Al powders (3-50 μm) were used as raw materials in fabricating Fe-Al<sub>2</sub>O<sub>3</sub> composites. To produce the composites having an Al<sub>2</sub>O<sub>3</sub> volume fraction of 40%, the powder mixture of Fe, Fe<sub>2</sub>O<sub>3</sub> and Al were prepared with their volume fractions derived from the reaction equation  $2\text{Al} + \text{Fe}_2\text{O}_3 \rightarrow \text{Al}_2\text{O}_3 + 2\text{Fe}$ . The weight ratio of Al, Fe<sub>2</sub>O<sub>3</sub> and Fe in the mixed powder is thus 10.48: 31.06: 58.50. The

\* Corresponding author: [zhg1200@sina.com](mailto:zhg1200@sina.com)

powder mix was ball-milled in a stainless steel vacuum jar for 2 h and compacted under a pressure of 180 MPa into cylindrical specimens with a diameter of 30 mm and a length of 5 mm. The cylindrical specimens were heated to a temperature above 1473 K in a vacuum furnace and then held at this temperature for 10 min before cooling down to room temperature inside the furnace. The composite samples were mechanically polished and investigated by using XRD (Rigaku D/MAX2400) and SEM (Quanta 2000) equipped with an energy dispersive spectroscopy (EDS).

## 2.2. Thermodynamic analysis

The layout of STA449C DSC thermal analyzer is similar to that of XD device shown in our previous paper[8]. When the temperature in the vacuum furnace of the DSC reaches critical values, chemical reactions take place in the powder mixture, in a manner similar to what occurs in the XD device. The mass of the sample placed in the DSC crucible is 5~15 mg cut from the cylindrical specimen, the environment and condition for the sample being tested in the DSC crucible are similar to those used in the XD furnace. Therefore, the DSC curve can be used to determine the temperatures at which the reactions between the Fe, Fe<sub>2</sub>O<sub>3</sub> and Al take place during the heating and cooling stage.

In order to obtain the DSC curves, the sample was heated in argon atmosphere in the furnace of STA449C thermal analyzer, wherein the temperature was increased from the ambient (298 K) to 1473 K at heating rates of 10, 20 and 30 K/min, respectively. Subsequently, the activation energies of the reactions occurring in the Al-Fe<sub>2</sub>O<sub>3</sub>-Fe system during the heating process were calculated and discussed.

## 3. RESULTS AND DISCUSSION

### 3.1 Activation energy

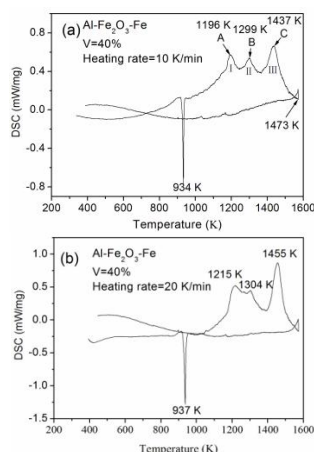


**Fig.1** DSC curves of the powder mixture generated at different heating rates: (a) 10 K/min, (b) 20 K/min and (c) 30 K/min.

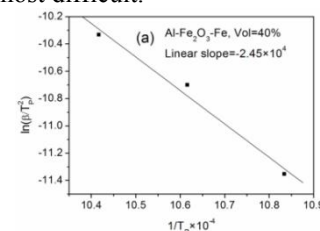
Activation energy (*E*) is the minimum amount of energy required for a chemical reaction to take place. It can be calculated by Kissinger equation [9]:

$$\frac{d\left(\ln\frac{\beta}{T_m^2}\right)}{d\left(\frac{1}{T_m}\right)} = -\frac{E}{R} \quad (1)$$

where *T<sub>m</sub>* is the temperature corresponding to the exothermic peak, *β* is the heating rate, and *R* is air constant (8.314 J/mol). As shown in Fig. 1a, three exothermic peaks appear at temperatures of 1196 (point A), 1299 (point B) and 1437 K (point C), respectively, during the heating process, meaning that the entire reaction of the Al-Fe<sub>2</sub>O<sub>3</sub>-Fe system are composed of three steps, designated here as step I, step II and step III. No peaks took place during the cooling stage, indicating that the reaction products are stable.

With the increase of the heating rate, all the exothermic reaction peaks shift towards higher temperatures (Fig. 1b,c). The reason is that when the heating rate increases, the rate of thermal energy input increases and the time available for reaction decreases. Transport of reactants (through diffusion), wetting, and final chemical reaction are all time-dependent processes. However, there is no sufficient time to improve the reaction conditions with increasing heating rates. Therefore, some of region would react at a higher temperature, resulting in the shifting of exothermic peaks to the higher temperature. According to the dependence of peak temperature on heating rate, the relation of  $\ln(\beta/T_m^2) \sim 1/T_m$  for each individual reaction is plotted in Fig. 2. By fitting data points using a straight line and setting its slope equal to  $-\frac{E}{R}$ , the

activation energies of the three reactions are calculated and found to be 203.8, 1110.5 and 380 kJ/mol, respectively. Consequently, step I is the easiest, while the step II is the most difficult.



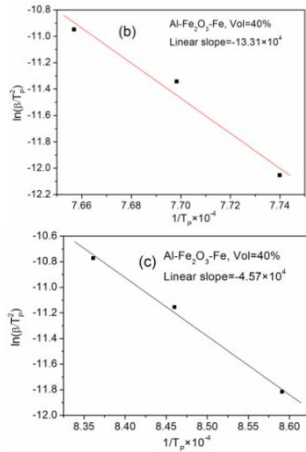


**Fig.2** Plots of the  $\ln(\beta/T_m^2) - 1/T_m$  of the three step reactions for the Al-Fe<sub>2</sub>O<sub>3</sub>-Fe system: (a) step I; (b) step II; (c) step III.

To understand the time-dependent behavior of reactions, the rate ( $\alpha$ ) of each of three steps was examined and compared (Fig. 3), by analyzing the DSC results obtained at the heating rate of 10 K/min [10]. All the three reactions exhibit a similar trend; that is, they start slowly, and then accelerate rapidly before becoming slow again [11]. Three steps took 456, 672 and 650 s, respectively. It can be seen from Fig. 3 that the reaction time of step II is the longest and its slope is also the smallest. Notably, the activation energy of step II reaction is also the highest among the three steps.

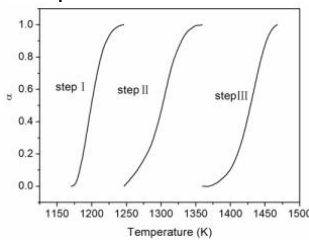


**Fig.3** Converting fraction ( $\alpha$ ) of the three steps reactions versus temperature at a heating rate of 10 K/min

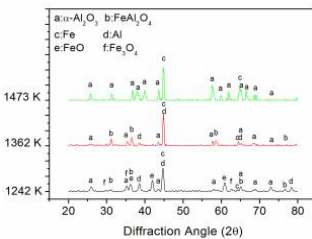


**Fig.4** XRD diffraction patterns of sintered products in Al-Fe<sub>2</sub>O<sub>3</sub>-Fe system

### 3.2 Intermediate reactions

In order to identify the nature of the transitional phases in the reaction, three green compacts were heated at the rate of 10 K/min up to temperatures at which the reactions occur, i.e., 1242, 1362 and 1473 K, respectively. Their corresponding XRD patterns are shown in Fig. 4. The composite resulting from the first reaction is found to comprise Al, Al<sub>2</sub>O<sub>3</sub>(s), FeO, Fe<sub>3</sub>O<sub>4</sub> and FeAl<sub>2</sub>O<sub>4</sub>. The SEM microphotograph of the composite is shown in Fig. 5a. EDS data of an intermediate phase FeO (labeled as A

in Fig. 5a) is shown in Fig.5b. Accordingly, the reaction for step I can be expressed as:  

$$4\text{Al(l)} + 12\text{Fe}_2\text{O}_3\text{(s)} = \text{Al}_2\text{O}_3\text{(s)} + 5\text{FeO(s)} + 6\text{Fe}_3\text{O}_4\text{(s)} + \text{FeAl}_2\text{O}_4\text{(s)} \quad (2)$$

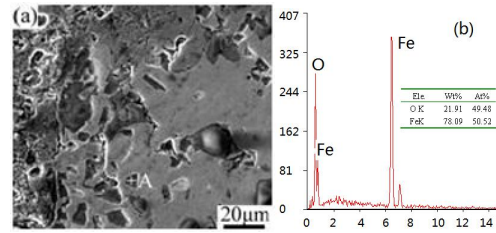


**Fig.5** SEM microphotograph (a) and EDS data (b) of the composites at heating temperature of 1242 K.

The variation of standard Gibbs free energy  $\Delta G_T^0$  of Equation 2 with temperature can be expressed as [12,13]:

$$\Delta G_T^0 = -1815365 - 176.9T \quad (3)$$

Note that  $\Delta G_T^0$  is less than zero for step I reaction, meaning it can take place spontaneously.

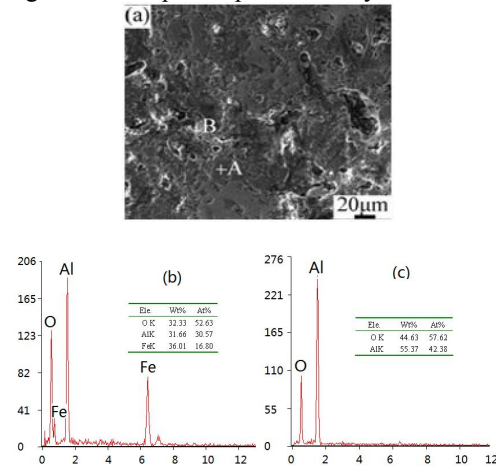


**Fig.6** SEM microphotograph (a) and EDS datum of the intermediate phase FeAl<sub>2</sub>O<sub>4</sub>(b) and stable phase Al<sub>2</sub>O<sub>3</sub>(c) from the composites at heating temperature of 1362 K.

When the heating was terminated at 1362 K, the resulting composite consists of Al, Al<sub>2</sub>O<sub>3</sub>, Fe and FeAl<sub>2</sub>O<sub>4</sub>(Fig.4). Its SEM microphotograph is shown in Fig. 6a. EDS data of the intermediate phases FeAl<sub>2</sub>O<sub>4</sub> and Al<sub>2</sub>O<sub>3</sub> (marked as A and B in Fig. 6a) are shown in Fig. 6b and 6c, respectively. Hence, the step II reaction can be written as:  

$$4\text{FeO(s)} + 3\text{Fe}_3\text{O}_4\text{(s)} + 10\text{Al(l)} = 4\text{Al}_2\text{O}_3\text{(s)} + 12\text{Fe(s)} + \text{FeAl}_2\text{O}_4\text{(s)} \quad (4)$$

It shows that the intermediate phases FeO and Fe<sub>3</sub>O<sub>4</sub> produced from step I reacted with Al to form the phases  $\alpha$ -Al<sub>2</sub>O<sub>3</sub> and FeAl<sub>2</sub>O<sub>4</sub>. The variation of standard Gibbs free energy  $\Delta G_T^0$  of Equation 4 as a function of temperature can be expressed as:

$$\Delta G_T^0 = -4233380 + 384.8T \quad (5)$$

Note that  $\Delta G_T^0$  is less than zero for step II reaction, meaning it can also take place spontaneously.

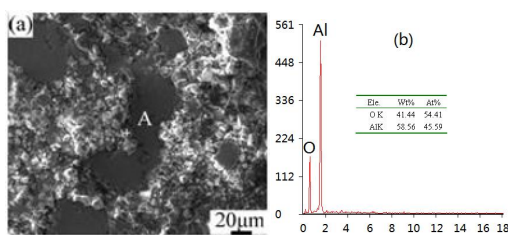
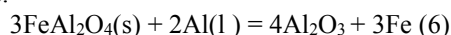


**Fig.7** SEM microphotograph (a) and EDS data (b) of the composites at heating temperature of 1473 K.

When the heating was terminated at 1473 K, the phases of the resultant composite consist of  $Al_2O_3$  and Fe (as seen in Fig.4). The SEM microphotograph of the composite is shown in Fig. 7a. EDS data of the stable phase  $Al_2O_3$  is labeled as A in Fig.7b. Hence, the stepIII reaction can be written as:



The intermediate phase  $FeAl_2O_4$  produced in previous steps reacted with Al in step III to form the phase  $\alpha-Al_2O_3$ . The variation of standard Gibbs free energy  $\Delta G_T^0$  of Equation 6 can be calculated according to:

$$\Delta G_T^0 = -774269 + 89.8T \quad (7)$$

Obviously,  $\Delta G_T^0$  is less than 0 for step III reaction, which means it can also take place spontaneously.

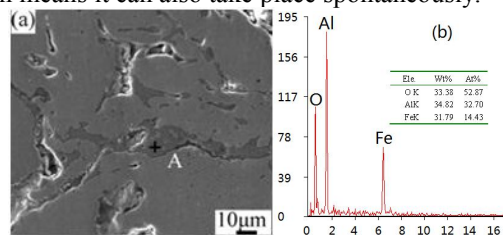


**Fig.8** SEM microphotograph (a) and EDS data (b) of the composites with reinforcement volume fraction of 10% at heating temperature of 1473 K.

Based upon the above analysis, when the starting materials with a composition of 10.48 wt% Al: 31.06 wt%  $Fe_2O_3$ : 58.50 wt% Fe are heated from room temperature to 1473 K, three step reactions occur, giving rise to three transitional phases, i.e., FeO,  $Fe_3O_4$  and  $FeAl_2O_4$ . Therefore, the heating temperature is an important factor that affects the combustion results. On the other hand, with a decrease in reinforcement volume fraction, the sum of the exothermic heat would be reduced, leading to a decline in combustion temperature. For example, when the reinforcement volume fraction is 10 vol%, the intermediate phase  $FeAl_2O_4$  remains in the final composite (Fig. 8).

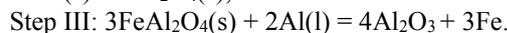
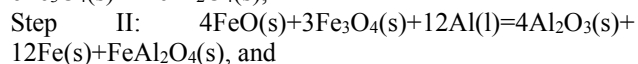
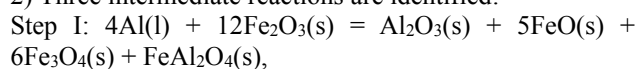
#### 4. CONCLUSIONS

*In situ* Fe- $Al_2O_3$  composites were fabricated from Al- $Fe_2O_3$ -Fe system by using XD method. Reaction mechanisms and process were investigated. The following conclusions can be drawn:

1) During the heating process, three exothermic peaks can be observed in the DSC curves of the Al- $Fe_2O_3$ -Fe system. There are no characteristic peaks during cooling process. With the increase of the heating rate, all the peaks moved

to higher temperatures.

2) Three intermediate reactions are identified:



3) The activation energies of the three reactions are calculated, which are 203.8, 1100.9 and 380 kJ/mol, respectively.

4) At a heating rate of 10 K/min, the times it took for the three reactions to complete are 456, 672 and 650 s, respectively. Their corresponding kinetic curves are similar, i.e., the reaction rate is very slow at the initial stage, and then it increases rapidly and, finally, it becomes slow again. Among the three reactions, the step II is the longest and also is the most difficult one.

#### ACKNOWLEDGEMENTS

This work was supported by the National Natural Science Foundations of China (No.51571118 and 51371098) and Natural Science Foundations of Jiangsu Province, China (No. BK20141308).

#### REFERENCES

- [1]Yudong Sui, Mojin Zhou, Journal of Alloys and Compounds, 2018, 741:1169-1174.
- [2]Bo Song, Zhiwei Wang, Qian Yan, Yuanjie Zhang, Yusheng Shi. Materials Science and Engineering: A, 2017,707: 478-487
- [3] Viseslava Rajkovic, Dusan Bozic, Aleksandar Devcerski, Milan T. Jovanovic. Materials Characterization, 2012, 67: 129 – 137.
- [4] Wen F, Lin T, Liu XQ. Processing Engineering, 2012, 27: 1738-1743.
- [5] Georgioua EP, Achanta S, Dostac S, Fernandez J, Matteazzi P, Kusinski J, Piticescu RR, Celis JP. Applied Surface Science, 2013, 275: 142-147.
- [6] Yaping Bai, Jiandong Xing, Haoliang Wu, Zhen Liu, Yimin Gao, Shengqiang Ma. Materials Design, 2012, 39: 211-219.
- [7] Babakhani A, Zahabi E, Yavari Mehrabani H. Journal of Alloys Compound, 2012, 514: 20-24.
- [8]ZhuHG, Dong K, Wang H, Li JL, Xie ZH. Powder Technology, 2013, 246: 456–461.
- [9] Zhang LC, XuJ, Eckert J. Journal of Applied Physical, 100: 033514.
- [10] Zhu HG, Min J, Li JL, Ai YL, Ge LQ, Wang HZ. Composite Science and Technology, 2010, 70 : 2183-2189.
- [11] Zhu HG, Jiang YL, Song JZ, Li JL, Paul Munroe, Xie ZH. Journal of Materials Science, 2013, 48: 929-935.
- [12] Ye DR, Hu JH. Hand book of thermodynamics data for inorganic substance. Beijing: Metallurgy Industry Press, 2002: 27-72.
- [13] Knacke O. Thermochemical properties of inorganic substances. Berlin: Springer-Verlag, 1991: 30-150.